Canadian Science Publishing | Transactions of the Canadian Society for Mechanical Engineering

A computational study on airflow balancing in a horticultural drying chamber

Journal:	*Transactions of the Canadian Society for Mechanical Engineering*
Manuscript ID	TCSME-2019-0016.R1
Manuscript Type:	Article
Date Submitted by the Author:	17-Apr-2019
Complete List of Authors:	El Halwagy, Mahmoud; Western University, Mechanical and Materials Engineering Straatman, Anthony; Western University Faculty of Engineering, Mechanical and Materials Engineering; Goyette, Bernard; Agriculture and Agri-Food Canada, Sherbrooke Research and Development Center Avigad, Gideon; Vineland Research and Innovation Centre, Research and Development
Keywords:	Flow balancing, Horticultural Chambers, Computational Fluid Dynamics (CFD), Porous Media, Food Refrigeration and Storage
Is the invited manuscript for consideration in a Special Issue? :	Not applicable (regular submission)

A computational study on airflow balancing in a horticultural drying chamber

Mahmoud Elhalwagy[1], Anthony Straatman[1+], Bernard Goyette[2] and Gideon Avigad[3]

[1]Department of Mechanical & Materials Engineering
Western University
London, Ontario, Canada, N6A 5B9
astraatman@eng.uwo.ca; tel: 519-661-2111, Ext. 88249

[2]Sherbrooke Research and Development Centre
Agriculture and Agri-Food Canada
Sherbrooke, Quebec, Canada, J1M 0C8

[3]Vineland Research and Innovation Centre
Vineland Station, Ontario, Canada, L0R 2E0

[+]Corresponding author

ABSTRACT

Simulations were conducted to study the airflow across skids of grapes in a Horticultural grape drying chamber for the purpose of balancing the airflow to produce a uniform drying environment. The focus of the study was on the approach taken to provide balanced airflow using a computational Fluid Dynamics (CFD) tool combined with experimental data. The process was to first characterize the crate stacks by comparison of airflow simulations across a single crate stack to experimental data to establish resistance coefficients. The next step was to use these coefficients to simulate a row of stacked skids to establish corrections in terms of additional (variable) resistance that would result in balanced airflow. The corrected model was then used to simulate flow through the entire horticultural chamber to confirm that under the conditions of fan operation, the balance of airflow persists. The study shows that while the unmodified stacks had nearly 20% imbalance from the first to the last stack, the stack with resistance modifiers corrected this imbalance to within 5%, which is considered suitable for operation of the chamber.

Key words: Flow balancing, Horticultural Chambers, Computational Fluid Dynamics (CFD), Porous Media, Food Refrigeration and Storage

1. INTRODUCTION

Food engineering is an increasingly important area of study. The processes of harvest, transportation and storage of produce, meat and different food products are important research topics in terms of maximizing the efficiency of food handling and increasing the shelf life of different foodstuffs. In terms of processing and storage, engineering tools like Computational Fluid Dynamics (CFD) are a means of simulation that can provide information required to design and optimize. The use of such tools in modern food engineering practice is important from both cost and time perspectives. It is not practical to develop and design climate-controlled processing systems and warehouses solely by experimentation and trial and error. In this manner, CFD is valuable since computational costs are much lower than the cost to conduct experiments; CFD can study numerous different parameters such that experiments are required in only a few key cases. CFD can be used to provide the detailed information required to predict flow patterns around produce/foodstuffs, balance airflows for storage and refrigeration, calculate heating/cooling loads for transportation; or give detailed information related to heat and mass transfer for predictions of moisture gain/loss, drying or respiration and metabolic processes. The present work is concerned with processing and storage of grapes.

Different Computational Fluid Dynamics (CFD) studies have been reported in the literature for flow predictions inside horticultural chambers, vehicles and storage facilities. One group gave full/part of their focus to predicting the air patterns around foodstuffs for different applications. Of these studies (Tassou and Xiang 1998) was aimed at enhancing the modeling capability by modeling buoyancy effects inside of storage containers. Other studies analyzed the effects of forced cooling, packaging, placement and stacking on respiration, heat and mass transfer during storage for potato beds (Xu and Burfoot 1999), cold stores (Chourasia and Goswami 2007), strawberry packages (Ferrua and Singh 2009) and grape packages and stacking (Delele et al. 2009). Hoang et al. (2000) focused on selection of an appropriate turbulence model to optimize the air circulation in a system that includes a fan/blower. The local effects of dehumidification during cooling and forming of ice was considered by Delele et al. 2009 while the establishment of the optimal flow rates for efficient cooling with minimum temperature stratification was considered in Defraeye et al. (2015) and Ambaw et al. (2016). The remaining study considered air patterns for the purpose of predicting local distributions in applications like delay of ripening using 1-MCP (Ambaw et al. 2014).

Another element that had the focus of researchers is the utilization of porous media modeling concepts for characterizing stacks or pallets of produce and food stuffs. This approach proves efficient in such simulations because it is often difficult or unnecessary to characterize each individual part or food element numerically in a CFD simulation. The level of resolution depends on whether it is sufficient to simply characterize the resistance to flow and/or heat and mass transfer due to the presence of the bodies of foodstuffs, or if it is necessary to consider detailed shape and stacking effects. In other words, it is often sufficient to scale up the flow over individual food elements by averaging over a large volume of the domain (or the entire domain). A mathematical averaging of the transport equations is utilized in these cases to volume-average the "porous" domain. The averaging process produces additional terms that characterize the influence of the food elements on the average flow and heat/mass transport. Coefficients in the closure terms must are determined either by experiment or by pore-level simulation to facilitate simulation using the volume-averaged approach. By simulation, a small representative domain of foodstuffs (a representative-elemental-volume (REV)) must be developed and then simulated from which results can be averaged to obtain the coefficients of closure (Dyck and Straatman 2015, Khan and Straatman 2016,

Elhalwagy et al. 2017). Alternatively, the closure coefficients can be obtained from experiments on small stacks of produce and using sensitivity analysis and final experimental evidence for verification (Alvarez and Flick 2007, Ambaw et al. 2013). While the first approach is systematic and general, it has some challenges in application; the actual representative characterization of produce geometrical shapes (e.g. grape bunches, bumpy-shaped strawberries, etc.), additional packaging (e.g. card boxes and wooden skids) and stacking effects are the most pronounced and they render the second choice more viable in most cases. It is also difficult to specify a general REV for analysis in a lot of cases as an REV has to be isotropic and physically representative at the same time (Elhalwagy et al. 2017).

In the present work, a conjugate CFD approach is utilized for simulating the airflow through stacks of grape-filled crates in a horticultural drying chamber for purpose of studying the airflow in the chamber and through the grape stacks. The objective of the study is to balance the airflow across rows of vertical stacks such that in operation the chamber will provide a uniform drying environment. The technique presented is unique and utilizes porous media modeling to characterize the stacks of filled crates and for the perforated covers used to achieve balanced flow through the stacks. The simulation tool used is ANSYS CFX (2015).

2. GEOMETRIC MODEL

The chamber under consideration was designed and patented (Goyette 2016) by Vineland Research and Innovation Center, Niagara Falls, Canada. The chamber (see Fig. 1) is comprised of a large rectangular container, which houses both the air-conditioning section (filtering, chilling, heating, dehumidification, fans) in the bottom left portion, and a large drying chamber. The drying chamber holds two long rows containing stacked crates of grapes situated symmetrically about the center aisle. Each row includes six vertical stacks, and each stack includes fifteen levels of five crates placed in the pattern shown in Fig. 2. Each stack is wrapped on it vertical sides with layers of plastic wrap such that the only path for airflow is vertically. As such, the stacks are treated as independent in terms of airflow; i.e. air does not flow from stack to stack. The connection between the air-conditioning section and the drying chamber consists of two circular air inlets where air is blown by axial fans down the center aisle of the chamber, and returns through two rectangular openings located at the floor. The vertical stacks of grapes are arranged such that the skids form a rectangular "duct" along the floor which is opened to the air-conditioning section at one end (through the rectangular openings) and closed at the other end such that the only entry for air is from the upper surface of the grape stacks. In operation, the fan system blows air down the center aisle through the circular air inlets, which sets up a suction in the air-conditioning section thereby drawing air from the rectangular openings connected to the stacks of grapes. Thus, air circulates from the chamber downward through the grape stacks, along the floor through the duct formed by the row of skids, and into the air-conditioning section where it is conditioned for temperature and humidity, mixed with some fresh air and then recycled back to the large chamber through the circular openings.

The current work focuses on CFD analysis of the airflow throughout the chamber to study the distribution of drying air. The airflow through the air-conditioning section of the system is not considered in this study. As such, the two circular air inlets and the rectangular returns are boundary surfaces, and the connection between the air-conditioning section and the drying chamber is made by imposing appropriate boundary conditions on these surfaces.

As the overall problem is complex and comprised of several different detailed features, the study on airflow balancing is conducted in 3 stages. In the first stage, experimental measurements of airflow through a stack of grape-filled crates are considered to establish coefficients that are then used to reduce the complex geometry of the grape crate stacks to simple rectangular prisms of porous media. In the second stage, computational simulations are conducted for one row of six vertical stacks to first establish the level of imbalance and then to develop a method to balance the airflow across the row. In the final stage, the entire chamber is modelled to illustrate the airflow in the drying chamber including the solution for flow balancing.

3. NUMERICAL MODELLING

Computational Fluid Dynamics (CFD) was used to simulate airflow in the present study. As it is airflow balancing that is sought, temperature effects are ignored and solutions are obtained by solving the continuity, momentum and turbulence (k-ε) equations in both fluid and porous regions for steady, incompressible, Newtonian flow of air, which is treated as an ideal gas. In the absence of external sources, the equations for continuity, momentum and turbulence may be simplified, respectively, in vector form as (Elhalwagy and Straatman 2017, Elhalwagy and Straatman 2018):

$$\rho(\nabla.\mathbf{v}) = 0 \tag{1}$$

$$\frac{\rho}{\phi}\nabla.(\mathbf{v}\,\mathbf{v}) = -\phi\,\nabla P + \nabla\left[\,\mu_e.\left(\nabla\,\mathbf{v} + (\nabla\,\mathbf{v})^T\right)\right] + \phi\,S_M \tag{2}$$

$$\nabla\,(\rho\,k\,\mathbf{v}) = \phi\,\nabla\left[\left(\mu + \frac{\mu_t}{\sigma_k}\right)\nabla k\right] + P_k - \phi\,\rho\,\varepsilon - \phi\,S_k \tag{3}$$

$$\nabla\,(\rho\,\varepsilon\,\mathbf{v}) = \phi\,\nabla\left[\left(\mu + \frac{\mu_t}{\sigma_\varepsilon}\right)\nabla\varepsilon\right] + C_{1\varepsilon}\,P_k\frac{\varepsilon}{k} - \phi C_{2\varepsilon}\,\rho\,\frac{\varepsilon^2}{k} - \phi\,S_\varepsilon \tag{4}$$

Here, the momentum equation is in its superficial (extrinsic) form and the turbulence equations in their interstitial or intrinsic form. ϕ is the porosity, S_M is the momentum isotropic loss due to the presence of porous media (CFX-ANSYS 2015) which is broken down in a subsequent section, μ_e is the effective air viscosity which is given by $\mu_e = \mu + \mu_t$, μ_t is the turbulent viscosity given by $\mu_t = C_\mu \rho \frac{k^2}{\varepsilon}$, P_k is the turbulence production term in its standard definition (CFX-ANSYS 2015) and C_μ,$C_{1\varepsilon}$,$C_{2\varepsilon}$,σ_k,σ_ε are turbulence constants set to their default values in CFX-ANSYS (2015). S_k and S_ε are turbulent sources due to the presence of Porous media and are assigned by CFX-ANSYS (2015). In the pure fluid regions, the above equations are reduced to their point form; i.e. $\phi = 1$ and S_M=S_k=S_ε=0. The commercial software ANSYS CFX (2015) is used to solve the governing equations for all simulations. CFX utilizes a finite-volume discretization scheme with a direct pressure-velocity coupling approach to solve the transport equations for mass and momentum in addition to turbulence (CFX-ANSYS 2015). A standard k-ε model is utilised with the use of scalable wall functions for all walls (CFX-ANSYS 2015). Second-order discretization is used in the present simulations for advection and diffusion of all transport equations.

4. AIRFLOW STUDY

4.1 Single stacks of grape crates

As stated in section 2., the stacks of grape-filled crates are to be modelled as porous regions and, therefore, require information on the permeability and inertial coefficients to quantify their influence in the momentum transport equations. Experimental data was available from Vineland Research (Goyette et al. 2013) characterizing pressure drop as a function of airflow rate from stacks of grape-filled crates. The single stack geometry considered in the experiments is shown in Fig. 3, which also includes an image of one filled crate. Note that the reduction from 5 crates per layer to one crate per layer was done to reduce the required airflow in the experiments to achieve the velocities encountered in the actual stack geometry. Though not shown in Figs. 2 and 3, the crates have a perforated base to allow air to flow freely through the stack of filled crates. The stack is wrapped on its vertical faces with a plastic sheath such that the only pathway for airflow is vertically through the crates. In the experiment, a small centrifugal blower draws air out of a rectangular plenum (Fig. 3) on which 15 filled crates are stacked. Operation of the blower produces a suction in the plenum, which draws air vertically downward from the upper exposed surface through the crate stack and into the plenum. As the bottom crate is supported by its edges, only the filled crates are considered for establishing the pressure drop; not the supporting skid (see Fig. 2), which is considered in the next stage of simulation as a collection duct that steers air drawn through the crate stacks to the air conditioning section. The pressure drop as a function of airflow rate from stacks of grape-filled crates was measured using a pressure meter Fluke™ model 922. The pressure meter has a measuring range of ± 4000 Pascals with a resolution of 1 Pascal and an accuracy of ± 1 %. Pressure data were obtained by measuring the static pressure difference between the plenum and a predetermined crate height. The airflow rate was measured at the outlet of the fan using a pitot tube according to the method described by ASHRAE (1997). Pressure measurements are obtained at 3 vertical positions along the crate stack (crates 4, 9 and 14 counted from the bottom) to confirm that the pressure profile is approximately linear (a departure from linearity would simply mean that the crates are not uniformly filled).

The net porosity of the filled crate stack was estimated to be 0.5 which, for the purpose of air balancing, turned out to be reasonable. The resistance to airflow in the crate stack was modeled using the Darcy-Forchheimer law, wherein momentum losses are characterized by expressions of the type:

$$S_{M,z} = -\frac{\mu}{K_{perm}}\mathbf{v}_z - K_{loss}\frac{\rho}{2}|\mathbf{v}|\mathbf{v}_z, \quad (5)$$

where K_{perm} and K_{loss} are the permeability and inertial loss coefficients, respectively, and are determined by comparison of experimental data across a range of flow velocities to CFD simulations with the resistance source term determined by Eq. 5. To get an initial realistic estimate of the porous resistance coefficients, a direct comparison of the measured pressure drop to the source term given in Eq. 5 was made; i.e. an assumption of pure Darcy-Forchheimer flow. The values derived by this comparison are K_{perm}= 7.5e-7 and K_{loss}= 4157. Minor tuning to these coefficients was then required to account for three dimensional effects and other deviations from pure Darcy-Forchheimer flow that are inherently accounted for in the CFD calculations. To facilitate this tuning, a CFD model consisting of a simple rectangular prism of the volume shown in Fig. 3 (not including the plenum) was discretized using simple grids of 2717 and 5724 hexahedral elements. Because of the simple one-directional flow, the predicted pressure drop from top to bottom was within 0.5% indicating that the results are grid-independent. The vertical faces of the domain were considered walls, while the upper surface was an inlet and the lower surface had a prescibed mass flow

based on bulk velocity. A series of calulations over the same range of velocities led to the modifed coefficients K_{perm}= 2.1e-07 and K_{loss}= 4760, which are very close to those derived from the initial estimate. A comparison of the measured data, the initial curve fit of Eq.5 and the CFD predictions using the modified coefficients is given in Fig. 4, which shows good correspondence particularly between the measured data and the experiments. Thus, the modified coefficients are used to characterize the crate stacks for all subsequent CFD calculations. Due to the extent of the crate itself, going from one to five crates per layer was not expected to change the flow structure.

4.2 Single row of grape stacks

In this stage the geometric model shown in Fig. 5a is considered, wherein 6 stacks of filled crates are arranged such that the skids on which they sit seal together to form a duct that is closed at one end and sealed to the return opening on the other. The computational domain is built in a conjugate framework, which is comprised of six porous regions (the stacks) and the fluid region inside the skids. In this manner, the inlet surface is the top of the stacks and the outlet surface is the end of the first skid, which in practice is the connection to the rectangular opening of the air-conditioning section. The contents of the stacks were modelled as porous media using the data established in Section 4.1. As noted, in practice the vertical edges of each stack are wrapped with plastic such that air can only flow vertically; there is no airflow allowed between the stacks. The region inside the skids is considered to be pure fluid (air). A fluid/porous interface was specified at the interface between the porous stacks and the area where air enters the hollow portion of the skid. The interface modeling in CFD is accounted for implicitly through the interface mathematics built into CFX-ANSYS (2015). On Fig. 5a, the fluid/porous interfaces are the 6 small areas at the bottom surface of each stack; this pattern is produced by subtracting the solid (wood) portion of the skid from the total skid volume. Note that while the stacks of crates are reduced to rectangular prisms of porous media, the geometric detail of the skids is preserved such that when put together the six skids form a "double-duct" with a ribbed upper surface where air drawn through the stacks gathers and flows to the air-conditioning section. Preserving the detail of the duct produced by the skid was considered important for balancing the airflow in the complete model. Figure 5b shows the computational mesh developed for the CFD simulations, which is comprised of 948,405 tetrahedral cells distributed such that near-wall regions and regions where flow complexity was expected has a higher density of cells. Simulations were also run on a mesh comprised of 523,296 tetrahedral elements to provide an assessment of the grid-independence. Results from the coarse and fine grids were within 0.5% based on pressure variations between the inlets and the outlet.

For the single row simulations, a velocity condition was set at the end of the first skid (the outlet) to produce suction across the stacks of crates, as opposed to using velocity-inlet and pressure outlets. This was considered to be the best way to mimic the airflow in the present case, wherein two fans produce suction in a plenum that draws air through the ends of skids sealed against the rectangular openings at the base. For the target airflow condition, the velocity imposed at the outlet was 15.24 m/s, which corresponds to 1920 l/s (4085 cfm) for the full row of stacks. This condition corresponds to the design condition for the selected fan system under the resistance estimated from the series of experiments conducted. An "opening" condition was set at the six inlet surfaces of the stacks. An opening condition requires an averaged pressure value and an estimate of turbulence intensity and length-scale, both of which were set to default values in CFX-ANSYS (2015). Wall conditions were set at all other surfaces of the domain. At a wall, the velocity

components go to zero, the pressure is found by extrapolation, and turbulence is estimated using scalable wall-functions.

A steady-state solution was obtained for the design condition, wherein convergence progressed monotonically to levels below 10^{-3}. Figure 6 shows (a) 3D streaklines through the stacks and skids, and (b) vertical velocities at the inlet of each stack in the row. Note that the pressure condition across the top of the stacks evolves uniformly based on the "opening" boundary condition. Figure 6a shows that the flow is drawn vertically through the stacks with no unexpected recirculations, collects in the duct formed by the skids and flows out of the outlet. The highest velocity is near the duct outlet, as expected, since the airflow collects from the farthest stack to the outlet. It is evident from the Fig. 6b that by having six identical stacks arranged in this manner, the relative airflow between the stacks in the row varies by more than 20% from the crate nearest the outlet to the last crate in the row, with the first crate having the highest airflow rate.

Two steps are taken to balance the airflow across the stacks. In the first step, the geometry was left as-is and the loss coefficients of the stacks were modified until airflow balance was achieved. Admittedly, this is not physically practical since it implies that the porous properties of the stacks can be changed, however, the process of trial and error required several computational runs and these could be carried out much more quickly on the simple stack model. A second step was to then convert these resistances into a practical solution, which involved placement of thin covers of specified permeability on the top surfaces of the stacks. Towards step 1, by the process of trial and error, the permeabilities listed in Table 1 were established to give nearly uniform airflow through the row of crate stacks. The table shows that the crate farthest from the outlet had the original values (K_{perm}= 2.1e-07, K_{loss}= 4760) meaning no further resistance was added, while each successive stack had a decreased permeability coefficient, with the lowest permeability assigned to stack 1. The inertial loss coefficient (K_{loss}) was kept constant for all of the stacks since it was just the net additional resistance that was sought in this step. Figure 7 shows the same plots as in Fig. 6, except using the loss coefficients given in Table 1. The plots indicate that the airflow is now balanced to better than 5% across the entire row of stacks.

Towards step 2, the relative resistances established in step 1 were used to compute the required resistance of a thin (0.0254m) cover of stiff foam board that could be laid on top of each of the crates after the chamber was loaded. The cover for each successive stack is different, and provides the additional resistance required to balance the flow across the entire row of crate stacks. The values for the loss coefficients of the covers are given in Table 2 and were obtained by simply matching the required pressure drop of the stacked crate to the thin layer to achieve a new permeability for a fixed inertial coefficient (K_{loss}= 4275). Once again, the value of the loss coefficient was fixed at an arbitrary value since it is only the net effect of the cover that is of interest at this point. Simulation results that include the thin, variable resistance covers is shown in Fig. 8, indicating that the variable covers produce the same balanced airflow distribution that was noted in Fig. 7. Note that for the simulations reported in Fig. 8, the loss coefficients for the crate stacks themselves were all the same (just as in Fig. 6); the only difference is that of the thin covers, which can be seen by close inspection of Fig. 8.

As a final task in step 2, the resistance across the covers now characterized in terms of loss coefficients was used to calculate the parameters of a perforated cover that could be constructed to achieve the required resistance to airflow for each stack. To this end, the calculator available at http://www.pressure-drop.mobi was used to compute the required clear area (surface porosity) of the thin cover based on the required pressure drop and flow velocity. The clear area was then used to compute the number of holes required in

the 1m x 1.2m cover and the spacing of the holes, assuming an even distribution across the cover. For simplicity, 12.7mm (0.5 inch) holes were assumed and the results for clear area, number of holes and hole spacing for the 5 covers is given in Table 3. No simulations were performed for the detailed perforated cover geometries as this would be prohibitively expensive computationally.

5. FULL CHAMBER SIMULATIONS

In this final stage of the study, simulations were conducted for the full drying chamber (see Fig. 9) using the design airflow rate to show the overall distribution of airflow and to give information on the pressure drop the fans are required to overcome for operation of the chamber. Once again, the crate stacks along the long walls are treated as wrapped such that each stack is a rectangular prism of porous media which functions independently between the chamber and the return duct formed by the skids. The rows of stacks in Fig. 9 are identical to that considered in section 4.2 and include the thin covers with loss coefficients as indicated in Table 2. Though the drying chamber is mainly symmetric about the center aisle, two pieces of equipment above the air-conditioning section (upper left) are included in the chamber, which render the geomtery non-symmetric and thus the entire chamber domain has been modelled and discretized. Fluid/porous interfaces are now also included at the surface that connects the upper surfaces of the stacks and the chamber. The exposed vertical surfaces of the stacks are considered as walls.

A velocity condition was set at the skid edge(s) just as in the single row calculations, but the inlet was now moved to the position of the the fan inlets (see Fig. 1), such that two jets of highly turbulent airflow are blown into the domain down the center aisle forming a positive pressure field in the chamber. The high turbulence was to simulate the fact that the jet was produced by an axial fan. Swirl profiles were free to evolve numerically as needed since the opening boundary condition in CFX-ANSYS (2015) specifies only average pressure value and develops the pressure profile freely. Despite the high turbulence at the inlet, the flow was mainly (nearly) laminar throughout the domain due to the low flow velocities. While the simulations provide information for velocity and pressure at all locations in the domain, the result of central interest in this study is the airflow distribution across the crate stacks in the two rows. Figures 10-11 show the computed results in terms of 3D streaklines. The figures show that the air jets produced by the axial fans are drawn upward by the suction produced at the upper surfaces of the crate stacks. The flow separates between the two rows of crate stacks and then spreads across the stack inlets by having portions of the upward flow continue towards the end stacks with the remainder being drawn backward towards the inlet planes. The pressure and velocity distributions across the upper surfaces of the stacks is shown in Figs. 12 and 13, respectively, where it is show that the velocity profiles across the stack is much more non-uniform than in the single-row simulations of section 4.2. Despite this variation at the upper surface, the airflow volume is still balanced to within 5% across the stack indicating that the approach used for balancing is viable.

6. SUMMARY

In this study, simulations were conducted to study the airflow across skids of grapes in a Horticulture grape drying chamber. The chamber was studied to understand the airflow distribution, and to balance the resulting airflow to produce a uniform drying environment. It was found that the arrangement of stacked crates had an imbalance of 20% in terms of volume flow rate of air at the design flow rate of the system. This imbalance was corrected by adding thin, variable-resistance covers to the tops of the stacked skids, where the highest additional resistance was required at the skid directly adjacent to the air-conditioning

section. The covers corrected the airflow imbalance to within approximately 5%, which is suitable considering the differences that may naturally occur across the grape-filled crates. The focus of this study was on the approach used to achieve the balanced air flow, which included reduction of the stack geometry to a rectangular prism of porous media, a study of the flow across a row of six stacks to establish the imbalance, correction of the imbalance by introducing thinn covers of specified resistance, and finally, simulation of the complete drying chamber to confirm that balanced flow exists at the design flow condition.

ACKNOWLEDGEMENTS

The authors would like to acknowledge the financial support from Vineland Research and Innovation Center, Niagara Falls, Canada

References

Alvarez, G. and Flick, D. 2007. Modelling turbulent flow and heat transfer using macro-porous media approach used to predict cooling kinetics of stack of food products. Journal of Food Engineering, **80**(2), 391-401.

Ambaw, A., Verboven, P., Defraeye, T., Tijskens, E., Schenk, A., Opara, U. L. and Nicolai, B. M. 2013. Porous medium modeling and parameter sensitivity analysis of 1-MCP distribution in boxes with apple fruit. Journal of Food Engineering, **119**(1), 13-21.

Ambaw, A., Verboven, P., Delele, M. A., Defraeye, T., Tijskens, E., Schenk, A. and Nicolai, B. M. 2014. CFD-based analysis of 1-MCP distribution in commercial cool store rooms: porous medium model application. Food and Bioprocess Technology, *7*(7), 1903-1916.

Ambaw, A., Bessemans, N., Gruyters, W., Gwanpua, S. G., Schenk, A., De Roeck, A. and Nicolai, B. M. 2016. Analysis of the spatiotemporal temperature fluctuations inside an apple cool store in response to energy use concerns. International Journal of Refrigeration, 66, 156-168.

ASHRAE. 1997. Measurement and Instruments. Fundamentals Handbook. American Society of Heating, Refrigerating and Air-Conditioning Engineers, Inc. Atlanta, Georgia. Chapter 14.

CFX-ANSYS, Copyright 2015.

Chourasia, M. K. and Goswami, T. K. 2007. Steady state CFD modeling of airflow, heat transfer and moisture loss in a commercial potato cold store. International Journal of Refrigeration, **30**(4), 672-689.

Defraeye, T., Cronjé, P., Verboven, P., Opara, U. L. and Nicolai, B. 2015. Exploring ambient loading of citrus fruit into reefer containers for cooling during marine transport using computational fluid dynamics. Postharvest Biology and Technology, **108**, 91-101.

Delele, M. A., Schenk, A., Ramon, H., Nicolaï, B. M. and Verboven, P. 2009. Evaluation of a chicory root cold store humidification system using computational fluid dynamics. Journal of food engineering, **94**(1), 110-121.

Delele, M. A., Ngcobo, M. E., Opara, U. L. and Meyer, C. J. 2013. Investigating the effects of table grape package components and stacking on airflow, heat and mass transfer using 3-D CFD modelling. Food and Bioprocess Technology, **6**(9), 2571-2585.

Dyck, N. J. and Straatman, A. G. 2015. A new approach to digital generation of spherical void phase porous media microstructures. International Journal of Heat and Mass Transfer, **81**, 470-477.

Elhalwagy, M., Dyck, N. and Straatman, A. 2017. Numerical simulation of gas respiration in produce processing and storage applications. Proceedings of the 25th. Annual conference of the CFD society of Canada, Windsor, Canada.

Elhalwagy, M. and Straatman, A. G. 2017. Dynamic coupling of phase-heat and mass transfer in porous media and conjugate fluid/porous domains. International Journal of Heat and Mass Transfer, **106**, 1270-1286.

Elhalwagy, M. 2018. Dynamics of the Phase Coupling for Flow, Heat and Mass Transfer in Conjugate Fluid/Porous Domains. PhD thesis, Western University, London, Canada.

Ferrua, M. J. and Singh, R. P. 2009. Modeling the forced-air cooling process of fresh strawberry packages, Part I: Numerical model. International Journal of Refrigeration, **32**(2), 335-348.

Goyette, B, Piché, M. and Cathline, K. 2013. Internal report, Vineland research and innovation center, Niagara Falls, Canada.

Goyette, B. 2016. U.S. Patent No. 9,526,261. Washington, DC: U.S. Patent and Trademark Office.

Hoang, M. L., Verboven, P., De Baerdemaeker, J. and Nicolaı, B. M. 2000. Analysis of the air flow in a cold store by means of computational fluid dynamics. International Journal of Refrigeration, **23**(2), 127-140.

Khan, F. A. and Straatman, A. G. 2016. Closure of a macroscopic turbulence and non-equilibrium turbulent heat and mass transfer model for a porous media comprised of randomly packed spheres. International Journal of Heat and Mass Transfer, 101, 1003-1015.

Pressure drop calculator for perforated plates: http://www.pressure-drop.mobi/1002.html.

Tassou, S. A. and Xiang, W. 1998. Modelling the environment within a wet air-cooled vegetable store. Journal of Food Engineering, **38**(2), 169-187.

Xu, Y. and Burfoot, D. 1999. Simulating the bulk storage of foodstuffs. Journal of food engineering, **39**(1), 23-29.

Table 1: Summary of loss coefficients to produce a balance flow across one row of skids of crate stacks at a total airflow rate of 1920 l/s (4085 cfm)

Stack Number (1 is nearest the outlet)	K_{perm}	K_{loss}
1	5.50e-08	4760
2	8.60e-08	4760
3	1.17e-07	4760
4	1.48e-07	4760
5	1.79e-07	4760
6	2.10e-07	4760

Table 2: Summary of coefficients used to produce a variable resistance cover, which produces a nearly uniform flow across a single row of crate stacks. The thin covers were simulated as porous layers of 0.0254m thickness.

Stack Number (1 is nearest the plenum)	K_{perm}	K_{loss}
1	9.21e-10	4275
2	1.81e-09	4275
3	3.50e-09	4275
4	6.72e-09	4275
5	1.64e-08	4275
6	2.5e-07	4760

Table 3: Perforated Plate parameterization for stack covers.

	Loss Coefficients		dP for 0.0254m layer		Perforation		Hole Spacing	
Stack	K_{perm}	K_{loss}	[Pa]	[mbar]	% Clear area	# holes	x [mm]	y [mm]
1	9.21E-10	4275	140.159	1.402	2.92	277	72.15	60.13
2	1.81E-09	4275	73.520	0.735	4	379	61.65	51.37
3	3.50E-09	4275	40.185	0.402	5.35	507	53.30	44.42
4	6.72E-09	4275	23.077	0.231	7	663	46.60	38.83
5	1.64E-08	4275	12.102	0.121	9.5	900	40.00	33.33
6	2.50E-07	4760	5.491	0.055				

List of Tables

Table 1: Summary of loss coefficients to produce a balance flow across one row of skids of crate stacks at a total airflow rate of 1920 l/s (4085 cfm)

Table 2: Summary of coefficients used to produce a variable resistance cover, which produces a nearly uniform flow across a single row of crate stacks. The thin covers were simulated as porous layers of 0.0254m thickness

Table 3: Perforated Plate parameterization for stack covers

List of Figures

Figure 1: Isometric wireframe view of the drying chamber showing important dimensions. Units are in meters.

Figure 2: A detailed view of an empty vertical stack of crates. Each stack contains 15 layers of crates for a total of 75 crates resting on a wooden skid. Units are in meters.

Figure 3: Illustration of the single-stack geometry used to measure the pressure drop across crate stacks (a), and a single crate filled with grapes. The stack shown in part (a) is comprised of 15 of the crates shown in part (b) for the experiments on airflow and pressure drop. Note that the crate stack was wrapped on the vertical faces to only permit airfolw in the vertical downward direction.

Figure 4: Plot comparing pressure drop as a function of airflow velocity from the experiments to 1D and CFD simulations considering a single crate stack shown in Fig. 3.

Figure 5: Geometric model of one row of stacks including skid geometry. The computational grid contains 950,000 cells. In image (a), blue arrows show the position of inlets. These arrows have heads on both ends indicating that the flow can either enter or leave the face. The black arrows show the position of the outlet and indicate that the flow can only exit the outlet face.

Figure 6: Streamlines (a) and velocity contour plots (b) for single row of skid stacks. The condition shown corresponds to a total airflow volume of 1920 l/s (4085 cfm) and the contour colors on the upper surfaces indicate that the downward velocity (and airflow rate) increases from right to left, with the highest flow rate being in the stack nearest the outlet (bottom left).

Figure 7: Plot for single row of skid stacks for the same condition indicated in Fig. 6. In this case, the loss coefficients shown in Table 2 were used to balance the airflow distribution and the colour on the upper surfaces of the stacks indicate that the airflow rate is approximately uniform.

Figure 8: Streaklines and contour plots for a single row of stacks of smartcrates for the conditions indicated in Figs. 6-7, except with a variable resistance layer placed across the inlet.

Figure 9: Geometric model for full chamber. The computational grid contains 3,020,000 cells concentrated towards interfaces between fluid-porous regions, and at all walls and exposed surfaces. In image (a), blue arrows show the position of inlets, black arrows show the position of the outlets, and green arrows show the position of the permeable interfaces between the porous and fluid regions. Porous/fluid interfaces are included at the upper surfaces of the skid stacks and over the openings where the stacks are placed on the skids, as more clearly seen in Figs. 1 and 5a.

Figure 10: Results of airflow simulations for full drying chamber (3D view). The results show 3D streaklines colored by velocity.

Figure 11: Centrplane view of 3D streaklines in half of full chamber simulations.

Figure 12: Pressure contours shown along the inlet of the rows of crate stacks in the full chamber simulations.

Figure 13: Vertical velocity contours along the inlet surfaces of the crate stacks.

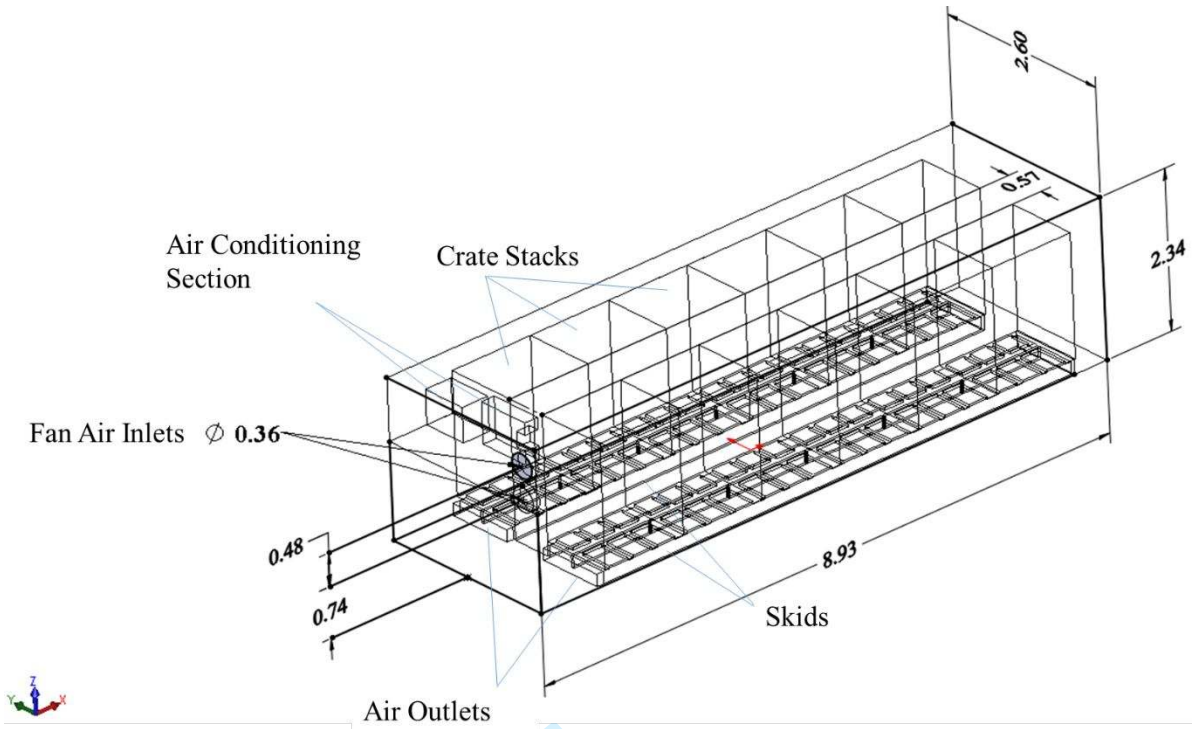

Figure 1: Isometric wireframe view of the drying chamber showing important dimensions. Units are in meters.

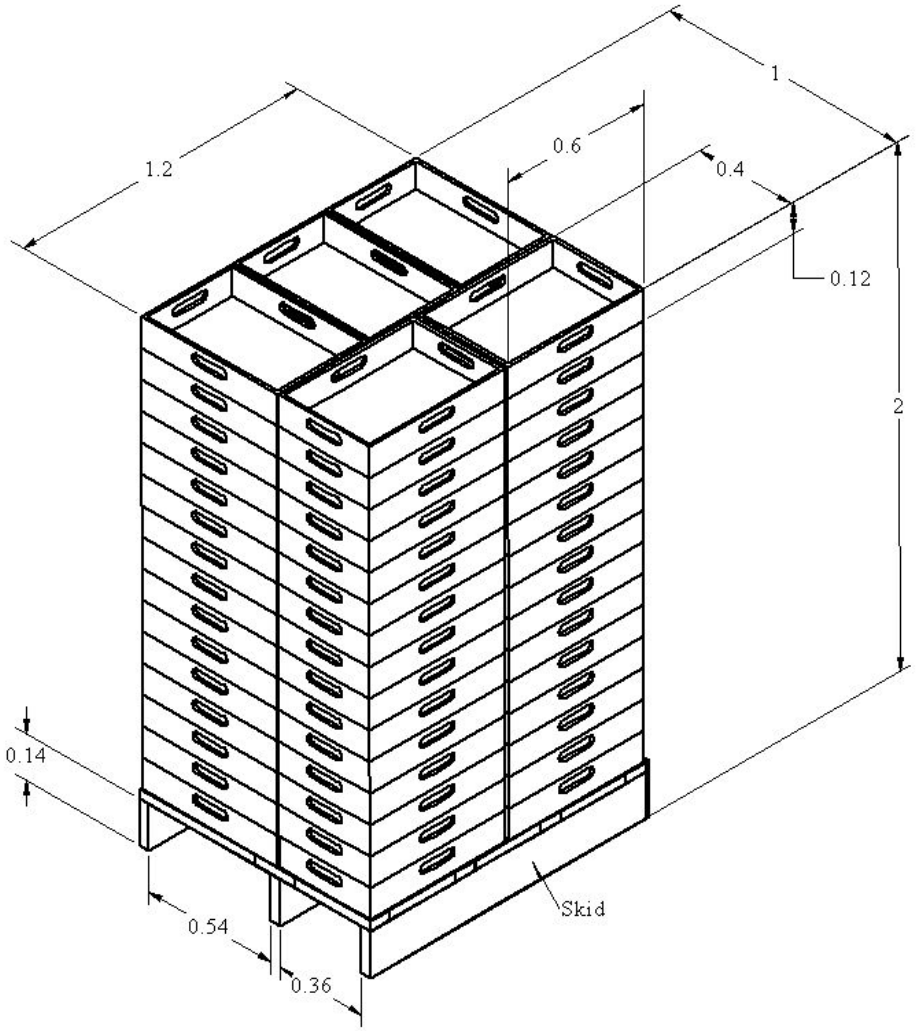

Figure 2: A detailed view of an empty vertical stack of crates. Each stack contains 15 layers of crates for a total of 75 crates resting on a wooden skid. Units are in meters.

(a) (b)

Figure 3: Illustration of the single-stack geometry used to measure the pressure drop across crate stacks (a), and a single crate filled with grapes. The stack shown in part (a) is comprised of 15 of the crates shown in part (b) for the experiments on airflow and pressure drop. Note that the crate stack was wrapped on the vertical faces to only permit airfolw in the vertical downward direction.

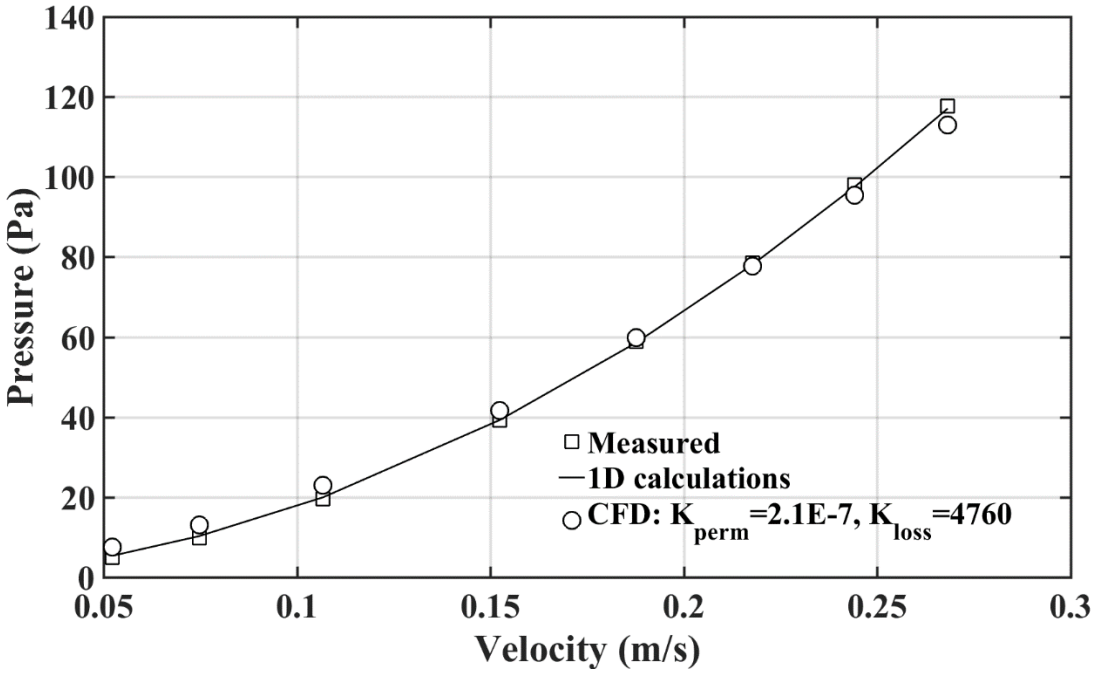

Figure 4: Plot comparing pressure drop as a function of airflow velocity from the experiments to 1D and CFD simulations considering a single crate stack shown in Fig. 3.

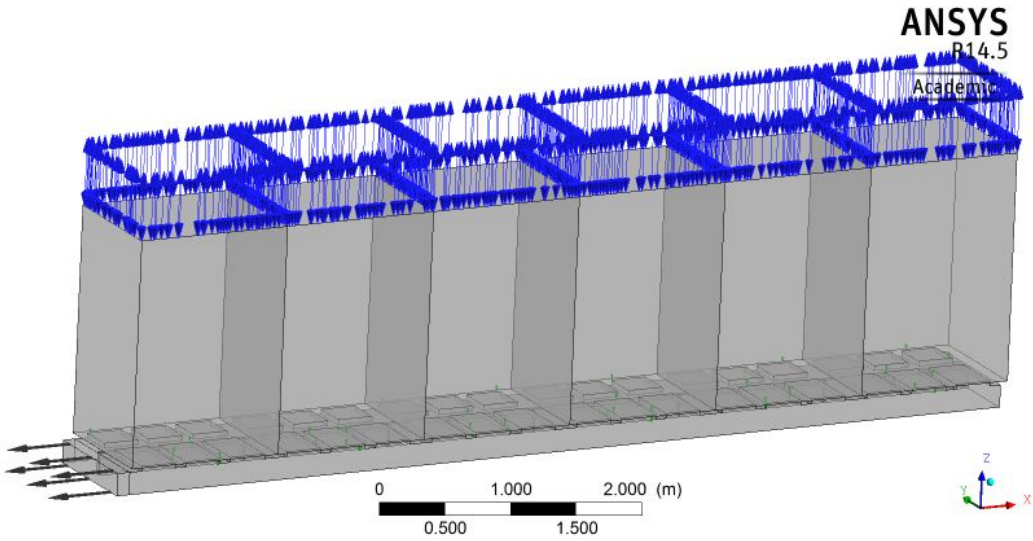

(a) Single-row stack geometric model

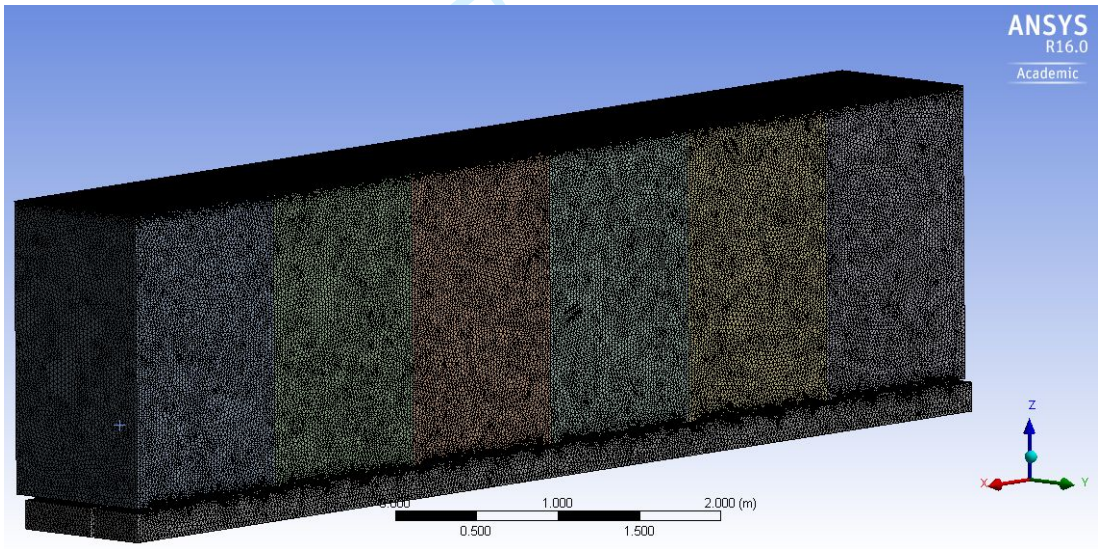

(b) Computational mesh for single-row stack geometric model

Figure 5: Geometric model of one row of stacks including skid geometry. The computational grid contains 950,000 cells. In image (a), blue arrows show the position of inlets. These arrows have heads on both ends indicating that the flow can either enter or leave the face. The black arrows show the position of the outlet and indicate that the flow can only exit the outlet face.

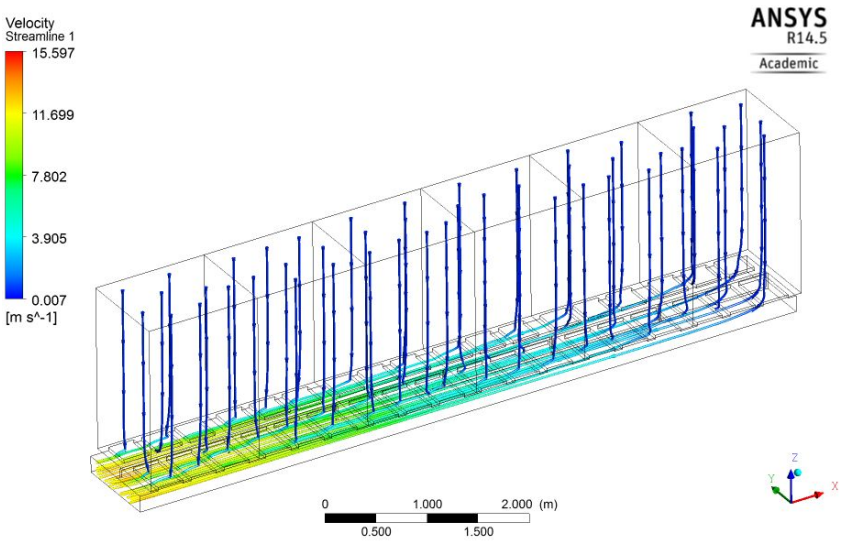

(a) Streamlines showing airflow direction and distribution,

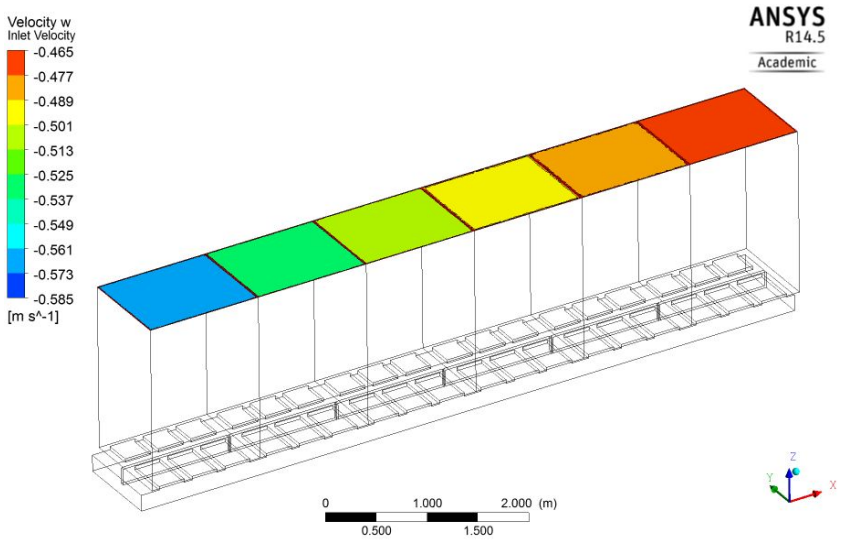

(b) Vertical (w) velocity on inlet plane of row

Figure 6: Streamlines (a) and velocity contour plots (b) for single row of skid stacks. The condition shown corresponds to a total airflow volume of 1920 l/s (4085 cfm) and the contour colors on the upper surfaces indicate that the downward velocity (and airflow rate) increases from right to left, with the highest flow rate being in the stack nearest the outlet (bottom left).

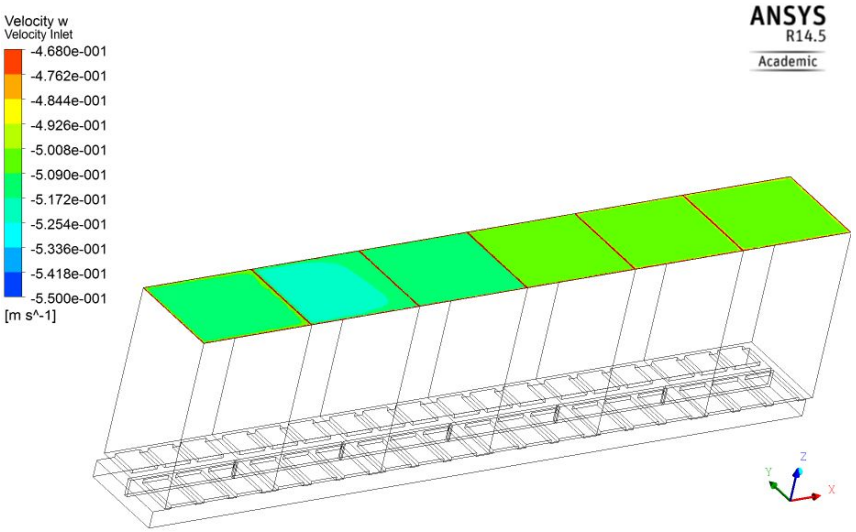

(a) Vertical (w) velocity on inlet plane of row

Figure 7: Plot for single row of skid stacks for the same condition indicated in Fig. 6. In this case, the loss coefficients shown in Table 2 were used to balance the airflow distribution and the colour on the upper surfaces of the stacks indicate that the airflow rate is approximately uniform.

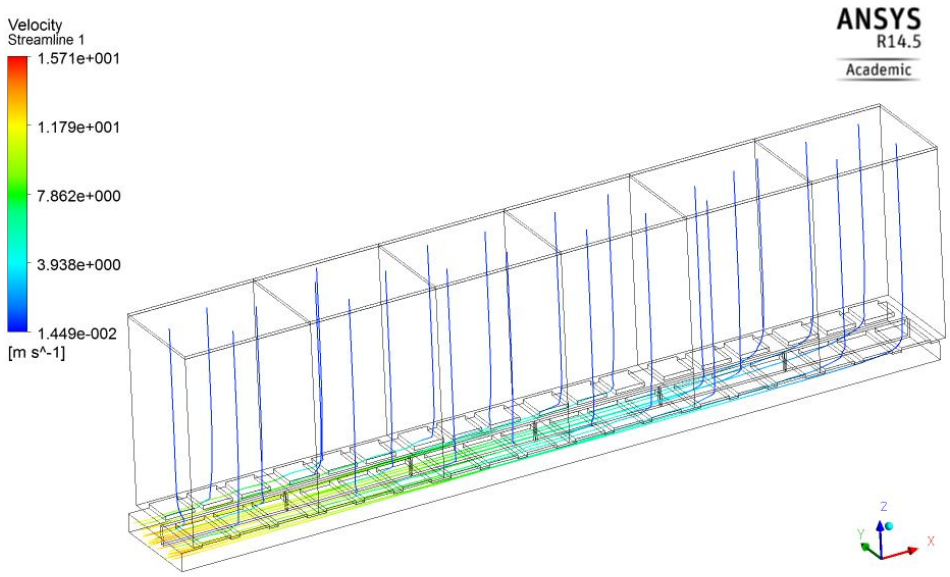

(a) Streamlines showing airflow distribution

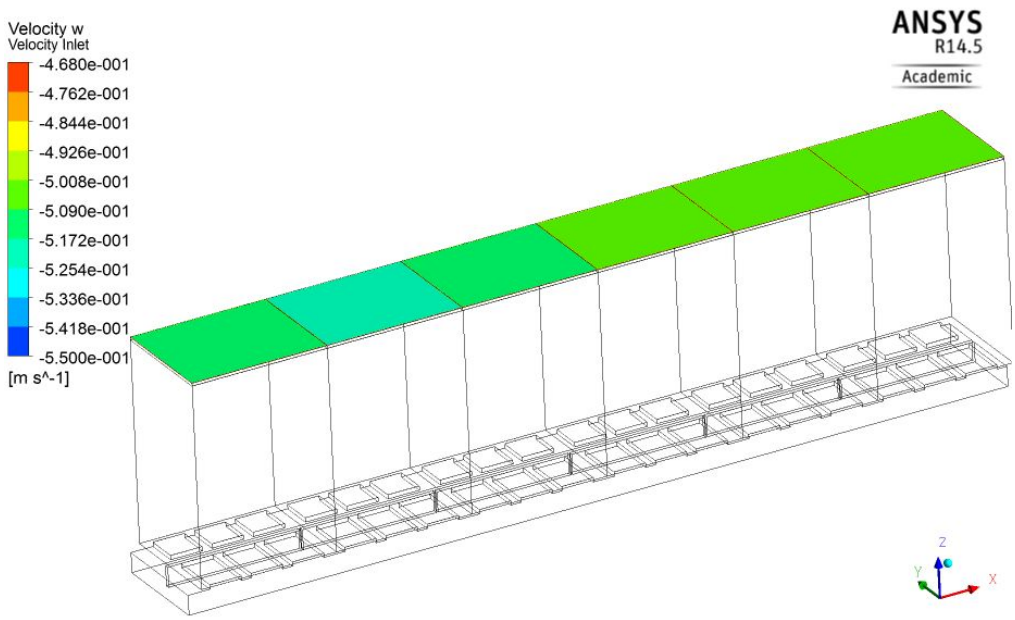

(b) Vertical (w) velocity on inlet plane of row

Figure 8: Streaklines and contour plots for a single row of stacks of smartcrates for the conditions indicated in Figs. 6-7, except with a variable resistance layer placed across the inlet.

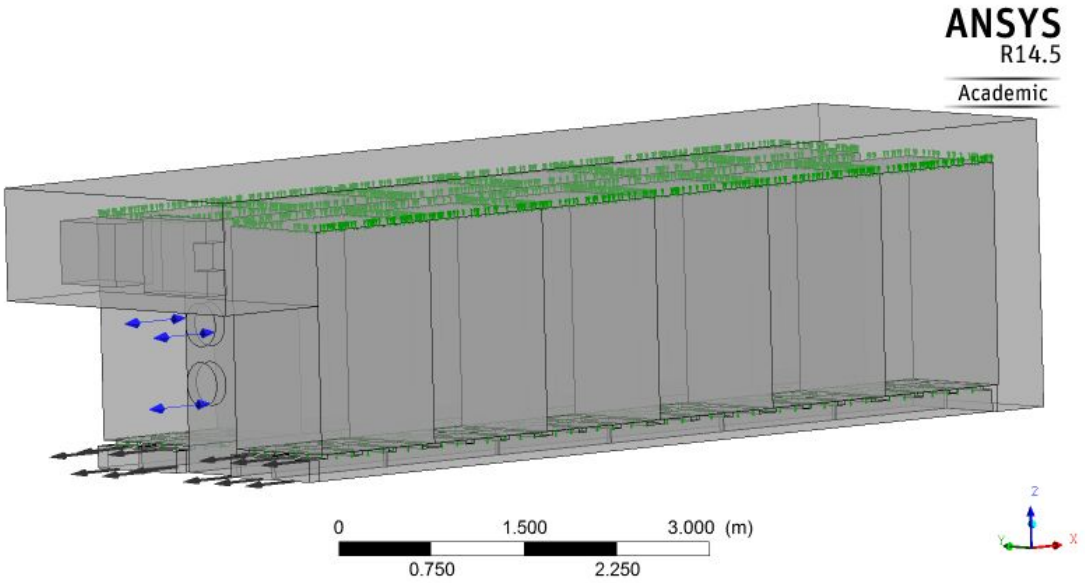

(a) Full-chamber geometric model

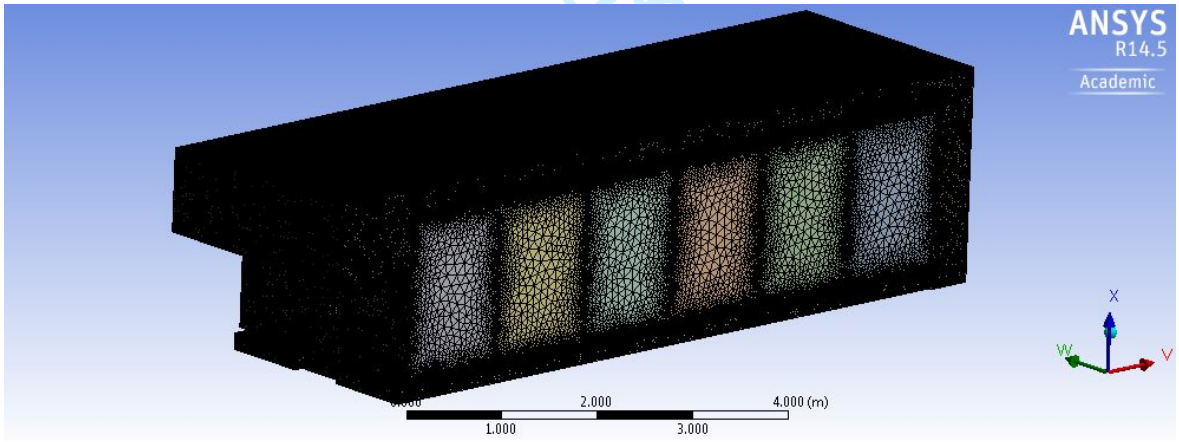

(b) Computational mesh for full-chamber geometry

Figure 9: Geometric model for full chamber. The computational grid contains 3,020,000 cells concentrated towards interfaces between fluid-porous regions, and at all walls and exposed surfaces. In image (a), blue arrows show the position of inlets, black arrows show the position of the outlets, and green arrows show the position of the permeable interfaces between the porous and fluid regions. Porous/fluid interfaces are included at the upper surfaces of the skid stacks and over the openings where the stacks are placed on the skids, as more clearly seen in Figs. 1 and 5a.

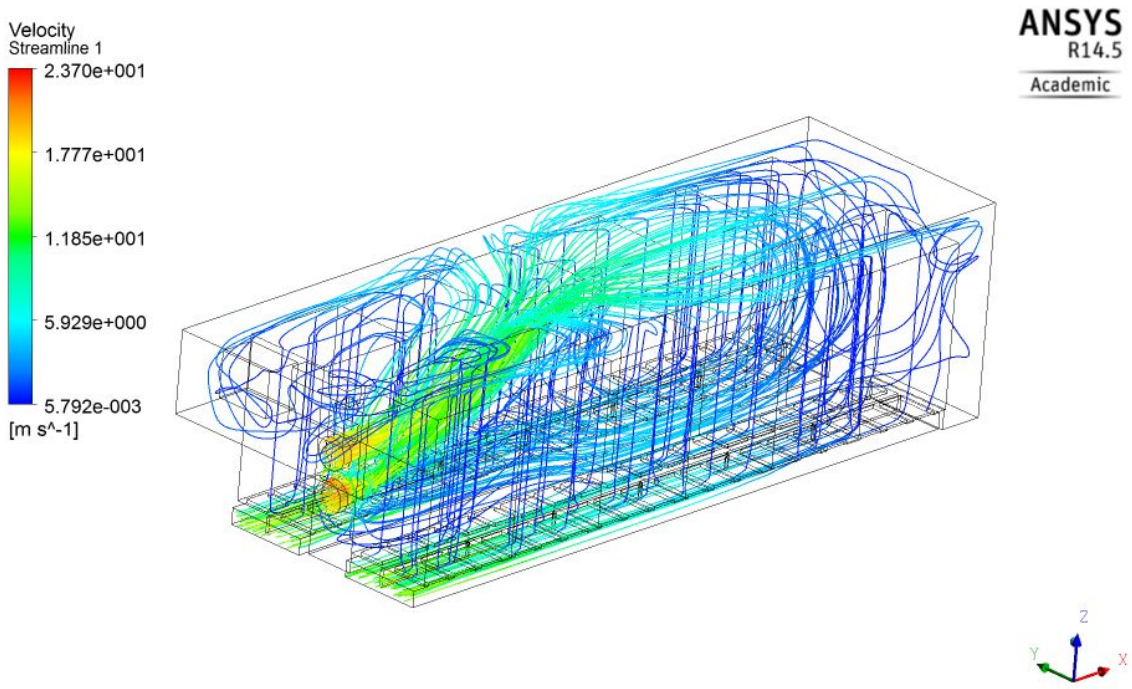

Figure 10: Results of airflow simulations for full drying chamber (3D view). The results show 3D streaklines colored by velocity.

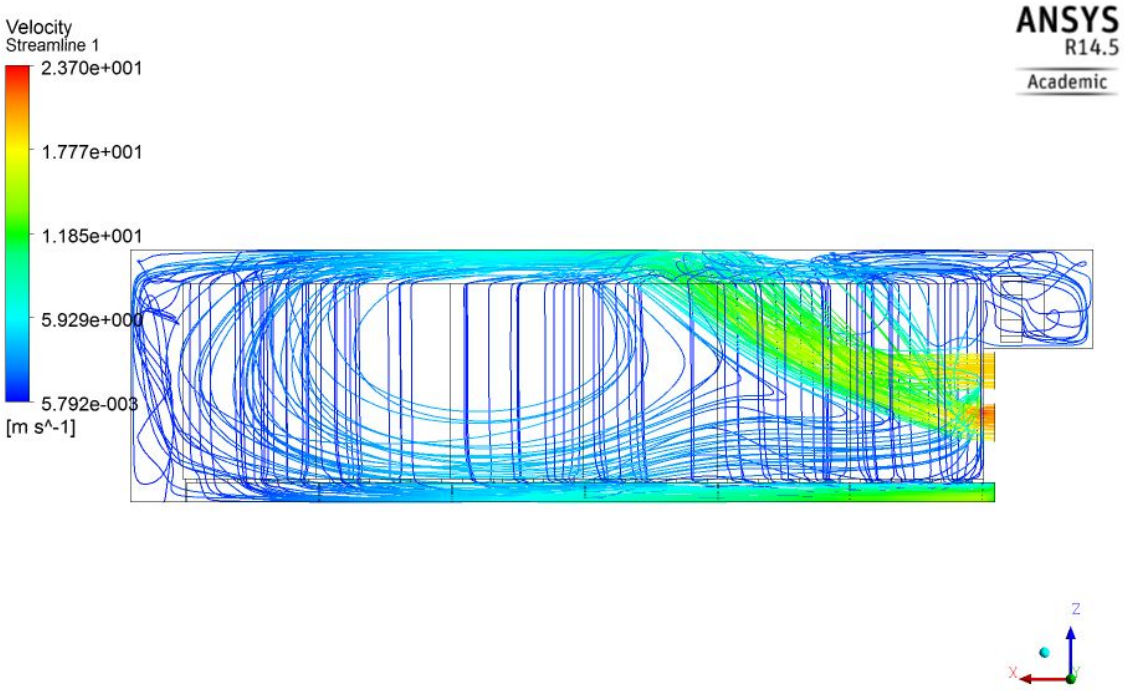

Figure 11: Centrplane view of 3D streaklines in half of full chamber simulations.

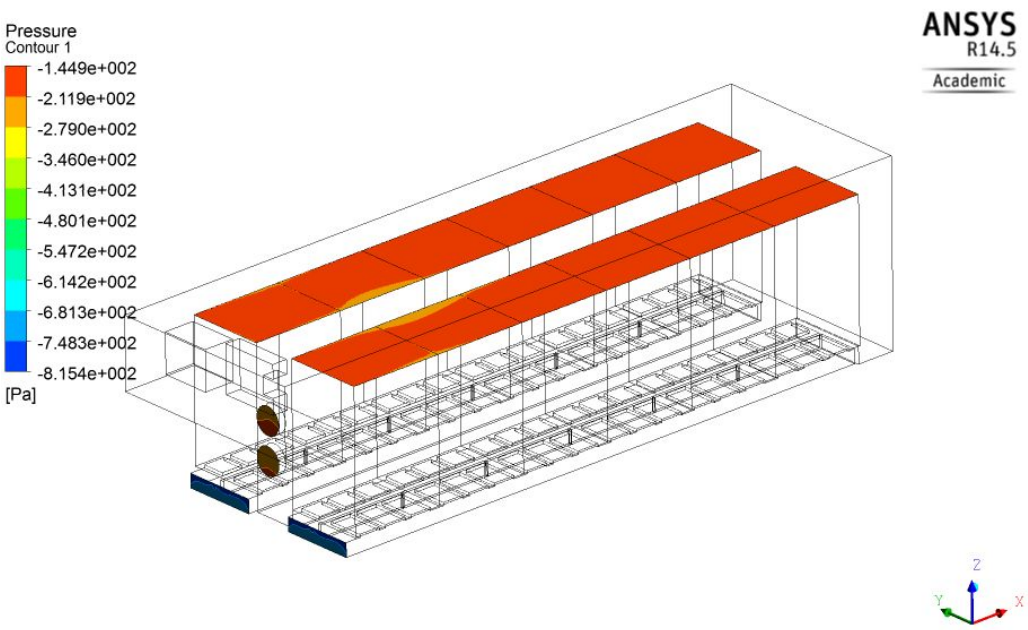

Figure 12: Pressure contours shown along the inlet of the rows of crate stacks in the full chamber simulations.

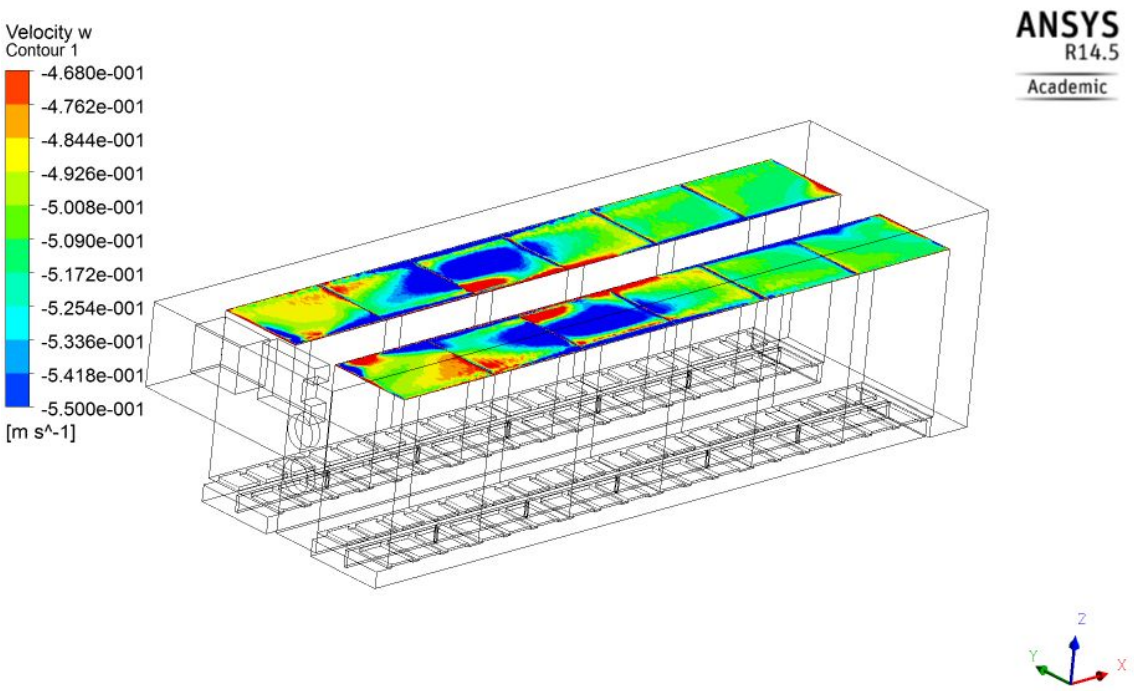

Figure 13: Vertical velocity contours along the inlet surfaces of the crate stacks.